

REPORT DOCUMENTATION PAGE				<i>Form Approved</i> OMB No. 0704-0188	
<p>The public reporting burden for this collection of information is estimated to average 1 hour per response, including the time for reviewing instructions, searching existing data sources, gathering and maintaining the data needed, and completing and reviewing the collection of information. Send comments regarding this burden estimate or any other aspect of this collection of information, including suggestions for reducing the burden, to Department of Defense, Executive Services, Directorate (0704-0188). Respondents should be aware that notwithstanding any other provision of law, no person shall be subject to any penalty for failing to comply with a collection of information if it does not display a currently valid OMB control number.</p> <p>PLEASE DO NOT RETURN YOUR FORM TO THE ABOVE ORGANIZATION.</p>					
1. REPORT DATE (DD-MM-YYYY) 06-02-2015		2. REPORT TYPE Final Performance		3. DATES COVERED (From - To) 30-09-2011 to 31-10-2014	
4. TITLE AND SUBTITLE Carbon Nanotube Thermoelectric Coolers				5a. CONTRACT NUMBER	
				5b. GRANT NUMBER FA9550-11-1-0311	
				5c. PROGRAM ELEMENT NUMBER	
6. AUTHOR(S) Serhii Shafraniuk				5d. PROJECT NUMBER	
				5e. TASK NUMBER	
				5f. WORK UNIT NUMBER	
7. PERFORMING ORGANIZATION NAME(S) AND ADDRESS(ES) NORTHWESTERN UNIVERSITY 633 CLARK ST EVANSTON EVANSTON, IL 60208-0001 US				8. PERFORMING ORGANIZATION REPORT NUMBER	
9. SPONSORING/MONITORING AGENCY NAME(S) AND ADDRESS(ES) AF Office of Scientific Research 875 N. Randolph St. Room 3112 Arlington, VA 22203				10. SPONSOR/MONITOR'S ACRONYM(S) AFOSR	
				11. SPONSOR/MONITOR'S REPORT NUMBER(S)	
12. DISTRIBUTION/AVAILABILITY STATEMENT A DISTRIBUTION UNLIMITED: PB Public Release					
13. SUPPLEMENTARY NOTES					
14. ABSTRACT The primary purpose of this project was studying of the thermoelectric Peltier cooling in carbon nanotube nano-circuits. The success of this work was based on strong coupling of the experimental and theoretical research. Thermoelectric effect was measured using two sequentially-connected carbon nanotube (CNT) field-effect transistors (FETs), each with charge carriers of opposite sign, either electrons or holes, whose concentration is controlled by the side gate electrodes. A change of the intrinsic temperature, T, inside the CNT owing to the thermoelectric effect is determined from the change of the position and width of spectral singularities manifested in the experimental curves of the source-drain electric conductance. Inside the central section of the carbon nanotube, we obtained an impressive Peltier cooling 57 K down from the liquid nitrogen temperature.					
15. SUBJECT TERMS carbon nanotube, thermoelectric cooling					
16. SECURITY CLASSIFICATION OF:			17. LIMITATION OF ABSTRACT	18. NUMBER OF PAGES	19a. NAME OF RESPONSIBLE PERSON Serhii Shafraniuk
a. REPORT	b. ABSTRACT	c. THIS PAGE			19b. TELEPHONE NUMBER (Include area code) 847-491-5453
U	U	U	UU		

The staff involved in the course of the project: S. Shafraniuk (PI, Research Associate Professor, theory and computer simulations), T. Gupta (graduate student, experimental fabrication of carbon nanotube Peltier coolers and their testing), I. P. Nevirkovets (Research Assistant Professor, experimental design and measurements of the carbon nanotube Peltier coolers), S. Davis (graduate student, experimental fabrication of carbon nanotube Peltier coolers and their testing), S. Mayle (graduate student, experimental fabrication and testing of the tunneling nano-thermometers), V. Chandrasekhar (Prof., consulting and providing access to fabricating and testing facilities).

Introduction. The primary purpose of this project was studying the thermoelectric Peltier cooling in carbon nanotube nano-circuits. Thermoelectric effect was measured [3] using two sequentially-connected carbon nanotube (CNT) field-effect transistors (FETs), each with charge carriers of opposite sign, either electrons or holes, whose concentration is controlled by the side gate electrodes. A change ΔT of the intrinsic temperature, T , inside the CNT owing to the thermoelectric effect is determined from the change

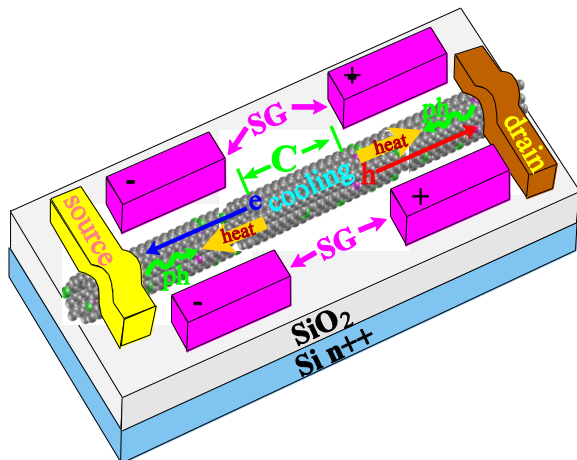


Fig. 1. Thermoelectric nano-circuit made of a single-wall carbon nanotube (CNT) forming two ambipolar field effect transistors which are connected electrically in sequence but thermally in parallel. The bias voltage is applied to CNT via source and drain electrodes which induce finite electric current. The pairs of side gate (SG) electrodes are setting the sign and concentration of charge carriers in the CNT, which are electrons on the left (blue arrow) and holes on the right (red arrow). Therefore, the electric current pulls the excitations out of the central region C. Pumping out of the electrons and holes from C de facto represents the Peltier cooling process. When the direction of the electric current is changed to opposite, the current pushes the electrons and holes toward the C region yielding its heating.

of the position and width of spectral singularities manifested in the experimental curves of the source-drain electric conductance. We deduced an impressive Peltier effect $\pm\Delta T \approx 57$ K inside the CNT associated with cooling and heating, depending on the direction of the electric current [3]. The effect can be utilized for building thermoelectric devices having a figure of merit up to $ZT_{\text{cold}} = 7.5 \gg 1$ and an appreciable cooling power density $P_{\text{cooling}} \sim 80$ kW/cm². Furthermore, we developed and tested the experimental approach to monitor intrinsic temperature on the nanoscale [5]. Monitoring of the intrinsic temperature and the thermal management are performed for the carbon nanotube (CNT) nano-circuits. The experimental results concerning fabricating and testing of the thermometer being able to monitor the intrinsic temperature on nanoscale are reported [5]. We also suggested a model describing a bi-metal multilayer system able to filter the heat flow, based on separating the electron and phonon components one from another [5]. The bi-metal multilayer structure minimizes the phonon component of the heat flow, while retaining the electronic part. The method allows one to improve the overall performance of the electronic nano-circuits due to minimizing of the energy leak. Besides, in this project, we studied other

approaches to highly efficient thermoelectric energy transformation using nanotube and monoatomic materials. This involved theoretical study of thermoelectricity in the nanoscale devices made of graphene and monoatomic layer dichalcogenides. The success of this work was based on strong coupling of the experimental and theoretical research.

Peltier cooling in carbon nanotube circuits. The central part of the work was the study of Peltier cooling in carbon nanotube thermoelectric circuits attracting a significant attention nowadays (DiSalvo 1999, Berber, Kwon et al. 2000, Small, Perez et al. 2003, Pop, Mann et al. 2007, Reddy, Jang et al. 2007, Bell 2008, Finch, Garcia-Suarez et al. 2009, Shafranuk 2009, Dubi and Di Ventra 2011). Systematic study of thermoelectric phenomena allows for better understanding of the intrinsic mechanisms of the energy

transformation and dissipation on the nanoscale. A bias electric voltage ΔV , applied to a conducting sample, pulls the charge carriers, thereby inducing a finite electric current $I_e = G_e \Delta V$, where G_e is the electric conductance. Since the bias voltage ΔV also induces an inhomogeneity of charge carrier density along the sample, it leads to a finite temperature difference $\Delta T = T_{\text{hot}} - T_{\text{cold}}$, where $T_{\text{hot(cold)}}$ is the temperature of the hot (cold) part of the sample. The thermoelectric effect is described as $\Delta V = S \Delta T$ where S is a linear-response, two-terminal property known as Seebeck coefficient.

Basic factors determining the efficiency of the thermoelectric process are illustrated with an expression for the figure of merit $ZT_{\text{cold}} = G_e S^2 T_{\text{cold}} / \Lambda$, where Λ is the heat conductance of the sample. Optimal selection of G_e , S and Λ represents the major challenge for the successful solution of the thermoelectric energy transformation problem. One can see that ZT_{cold} is improved for large magnitudes of the electric conductance G_e and Seebeck coefficient S , by simultaneously reducing the thermal conductance Λ to a lowest possible value. Current thermoelectric solutions still fall short in practical implementations, since the figure of merit of available nano-circuits is below the desirable threshold $ZT_c < 4$.

We report about an experimental observation of a large thermoelectric effect with the figure of merit up to $ZT_c \approx 7.5 \gg 1$ in the CNT nano-circuit formed by two field-effect transistors connected in series, utilizing the charge carriers of opposite polarity, either electrons or holes. The setup ensures an appreciable efficiency of the thermoelectric effect. The key element of exploited thermoelectric nano-circuit is a single-wall carbon nanotube, enclosed between the two pairs of the side-gate electrodes (SG), which control the sign and concentration of the charge carriers locally, thereby forming a step-wise electric potential $V_{\text{SG}}(x)$ on CNT (see Fig. 1a). The side gates are used to define the step-wise dependence of the electrochemical potential $\mu(x)$ versus coordinate x inside the CNT, as shown in Fig. 2a. The sign and concentration of the charge carriers in the left- and right-hand sections of the same nanotube is controlled electrically as shown in Fig. 2. The bias voltage ΔV is applied to the nanotube via source (S) and drain (D) electrodes. The sign of the thermoelectric effect (either cooling or heating) depends on the direction of electric current as illustrated by the diagrams shown in Figs. 2 a-c.

The two carbon nanotube field-effect transistors (FETs) forming the thermoelectric nano-circuit are connected electrically in sequence but thermally in parallel (Shafranjuk 2009). The thermal conductance of the carbon nanotube, Λ , is associated with the transport of electrons (e) and phonons (ph) as $\Lambda = \Lambda_e + \Lambda_{ph}$. Typically, $\Lambda_{ph} / \Lambda_e \sim 10^3 - 10^4$ (Berber, Kwon et al. 2000, Small, Perez et al. 2003, Pop, Mann et al. 2007, Shafranjuk 2009), and thus $\Lambda = \Lambda_{ph} \gg \Lambda_e$. The semiconducting carbon nanotube, implemented in our nano-circuit, has appreciable values of G_e and S (Small, Perez et al. 2003). A large value of the thermal conductance, $\Lambda_{\text{CNT}} = 100 - 3000 \text{ W}/(\text{K m})$, poses a well-known disadvantage [see Refs. (Berber, Kwon et al. 2000, Small, Perez et al. 2003, Pop, Mann et al. 2007, Shafranjuk 2009)] of carbon nanotubes when using them as elements of thermoelectric nano-circuits, because it hinders conversion of the heat energy into the electricity, thus limiting the performance of the CNT thermoelectric nano-circuits. The basic physical mechanisms reducing efficiency of the thermoelectric CNT nano-circuits - the backflow transport of phonons and the phonon drag - were studied in Refs. (Shafranjuk 2009) (Shafranjuk 2014).

In our work, aiming to minimize the negative impact of the phonon transport, we have used a

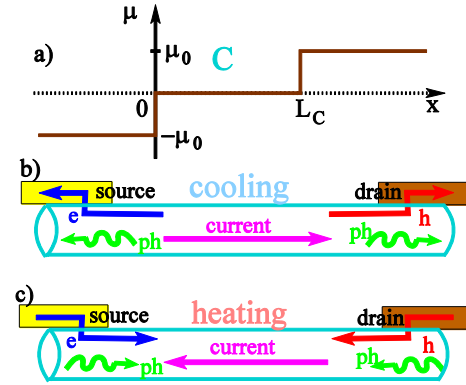


Fig. 2. (a) The coordinate dependence of the electrochemical potential $\mu(x)$ induced by applying the inhomogeneous side gate potential along the nanotube. (b) The cooling cycle: The electric current pulls out the electron and hole excitations from the central region of the nanotube. (c) The heating cycle: The electric current pushes the electrically charged excitations toward the central region.

special geometry of the nano-circuit by fabricating the source and drain Ti/CNT contacts with geometrical dimensions L_j smaller than the phonon mean free path l_{ph} : $L_j \leq l_{ph}$. To estimate l_{ph} , we use a condition $l_{ph}^{-1} \approx l_{pe}^{-1} + l_{pd}^{-1} + L_{CNT}^{-1}$, where l_{pe} and l_{pd} are the mean free paths of phonons due to scattering on electrons and defects, respectively. In our experiment $L_j \approx 0.5 \mu\text{m}$, $l_{pe} \approx 50 \mu\text{m}$, and $l_{pd} \gg l_{pe}$. Additional reduction of Λ is achieved by implementing a double-contact setup Ti/CNT/Ti where a high electric conductance is accompanied by a relatively low value of the thermal conductance for the same Ti/CNT-interface. In the Ti/CNT/Ti double-contact nano-circuit, the transmission probability $T_{Ti/CNT}^e$ through the Ti/CNT interface is considerable for electrons (and holes), whereas the interface transparency $T_{Ti/CNT}^{ph}$ for the phonons is very low, i.e., $T_{Ti/CNT}^{ph} \ll 1$, although propagation of the phonons inside the CNT is nearly ballistic. This happens because redirection of the phonons from CNT to Ti is accompanied by a significant change of the phonon momentum $\Delta\mathbf{q} = \hat{\mathbf{y}}q_y - \hat{\mathbf{x}}q_x$, where q_x and q_y are the phonon momentum components along the CNT axis and perpendicular to the Ti/CNT-interface, respectively (Shafranjuk 2009) (Shafranjuk 2014). Another reason why $T_{Ti/CNT}^{ph} \ll 1$ is because the phonon spectra of CNT and Ti are very distinct, and their misalignment reduces the phonon transmission through the Ti/CNT-interface considerably (Shafranjuk 2009) (Shafranjuk 2014). Therefore, for the sake of simplicity, we neglect transmission of the phonons between Ti and CNT by setting $T_{Ti/CNT}^{ph} \approx 0$. Because the phonons are effectively eliminated from the thermal transport in our thermoelectric nano-circuit, the resultant thermal conductance Λ is therefore remarkably low, i.e., $\Lambda = (\Lambda_{CNT}^{-1} + 2\Lambda_{Ti/CNT}^{-1})^{-1} \approx \Lambda_{Ti/CNT} / 2 \ll \Lambda_{CNT}$. The condition $\Lambda \ll \Lambda_{CNT}$ is observed because the phonons propagate mostly along the nanotube axis, bouncing back and forth from the ends of the short nanotube, thus providing no visible contribution to ZT_{cold} of the whole nano-circuit. On the contrary, the electrons and holes easily propagate between the metallic source and drain electrodes, which essentially causes the thermoelectric effect (see Figs. 2b,c). Since the phonons are effectively eliminated from the thermal transport, the overall thermal conductance Λ of the whole setup shown in Fig. 1 is by three to four orders of magnitude smaller as compared to the known value for the single-wall carbon nanotubes $\Lambda_{CNT} = 100 - 3000 \text{ W}/(\text{K} \cdot \text{m})$. It allows one to achieve a considerable increase of the figure of merit ZT_c in the setup shown in Fig. 1.

Table 1. The experimental parameters used to grow nanotubes and the variations produced by the different growth methods.

Growth Temp. (°C)	CH ₄ flow (sccm)	H ₂ flow (sccm)	Argon flow (sccm)	Comment
900	900	140	100	Usual method, long tubes
800	450	70	50	Growth is similar to 900 °C condition
700	450	70	50	Shorter tubes and low density
1000	100	350	0	cm-long straight tubes

Experimental observation of the Peltier cooling in the CNT nano-circuits. Next we consider the details of the experiment. The carbon nanotubes were grown in a chemical vapor deposition (CVD) using an optimized catalyst and annealing process. The catalyst consists of $\text{Fe}(\text{NO}_3)_3 \cdot 6\text{H}_2\text{O}$ (0.2 g) and Alumina nano-particles (5 nm, 0.4 g) in 10 ml of deionized water. The substrates, p-doped silicon with a 300 nm or 1 μm thermal oxide layer, are then dipped in the solution such that only a thin layer of solution is left on the substrate edge. Traditionally, the catalyst solution is spun onto the substrate; we have found that while this yields a large number of tubes they are densely packed and curved, thus being unsuitable for nano-fabrication. The dipping method, however, yields a low to moderate density of tubes, depending strongly on the concentration of FeNO_3 in the solution. We position the substrate inside the CVD in such a way that the catalyst dipped edge is perpendicular to the flow of gases. This is done so as to get the tubes to fall in the catalyst-free region of the substrate.

CNTs grown at higher temperature are usually linear and their size can go up to a few centimeters in length. Hence, they are ideal for fabricating of nano-circuits. During the early stages of fabrication, our focus was to find nanotubes which had ambipolar field-effect transistor (FET) behavior and low interface resistance. Summary of the CNT growth conditions used in the experiments is given in Table 1.

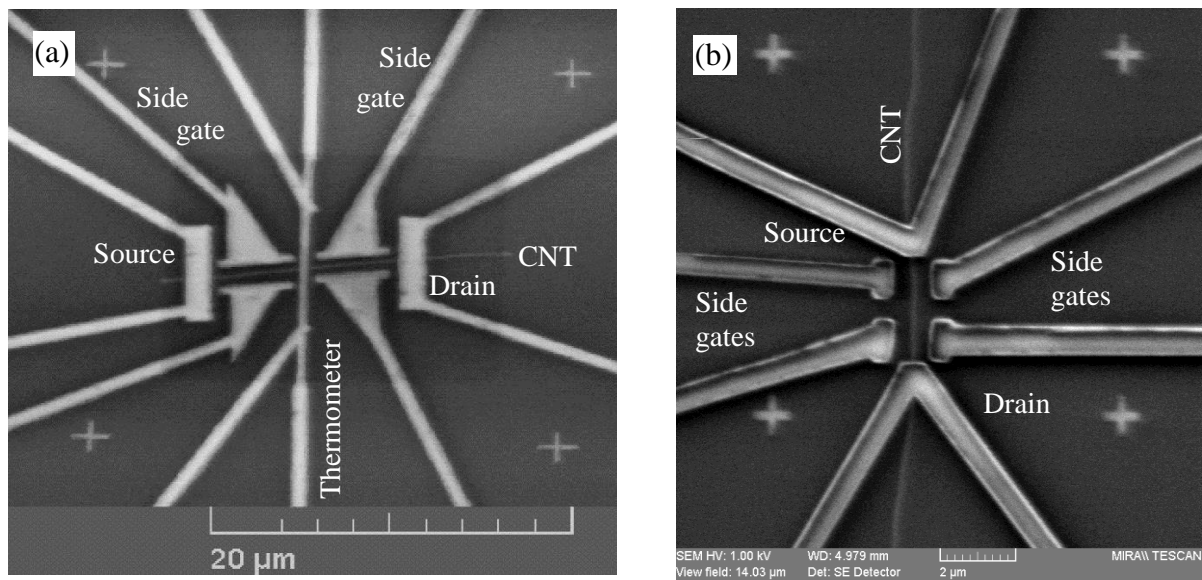


Fig. 3. SEM images of typical CNT nano-circuits used in the experiments. Side gates are employed to apply an electric field to the CNT.

The nanotubes were first characterized using both AFM and SEM techniques. From these measurements, and from electric characterization, we determined that the nanotubes grown at 900 $^{\circ}\text{C}$ were semiconductor-like. The CNT thermoelectric nano-circuits were fabricated using conventional electron beam lithography on a single CNT, thin-film metal deposition, and lift-off. SEM images of typical fabricated structures are shown in Fig. 3. The main nano-circuit consists of the central wire, which acts as a lead at the center of the nano-circuits. The side gates are fabricated parallel to the CNT, and spaced nominally 300 to 400 nm from the tube. Finally, along the tube itself, a conventional four-probe structure is fabricated in order to both characterize the tube and drive the thermoelectric circuit. After all of the structures are fabricated and connected to larger bonding pads, the area surrounding the tube, which is protected via resist, is cleaned of any

stray tubes using oxygen etching. This is done to ensure that the side gates are not shorted to the device. The thermometer, also fabricated in some cases (cf. Fig. 3a), is supposed to be a tunnel junction whose conductance is dependent on temperature. Its development is still in progress, so in this paper we use indirect temperature measurement as described below.

In the first nano-circuits, we used Pd electrodes deposited via electron beam evaporation in a high-vacuum chamber with a base pressure of $5 \cdot 10^{-7}$ Torr. With palladium contacts, the interface resistance was around 20 k Ω which went down even further on annealing at 230 °C for half an hour. With these contacts, the on-state conductance G/G_0 (where $G_0 = 7.75 \cdot 10^{-5}$ S is the conductance quantum) was around 0.024, whereas the off-state conductance was negligible as shown Fig. 4. Such FET's only showed p-type conductance. The reason for this is most likely that these CNT's have higher band gaps and we are not able to reach into n-type conductance regime.

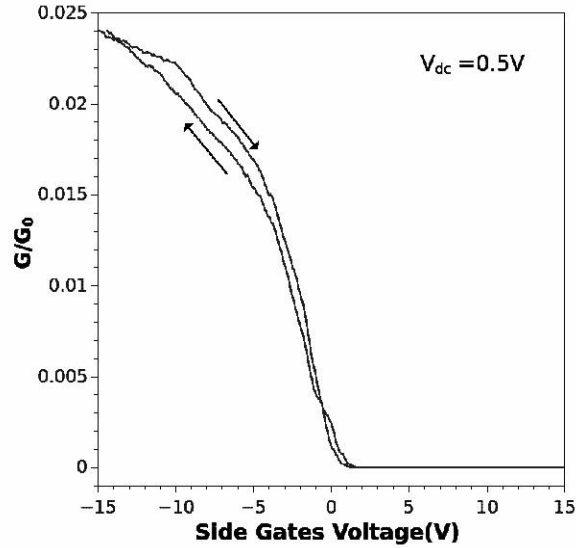


Fig. 4. Normalized conductance vs. side gates voltage dependence at a bias voltage $V_{dc} = 0.5$ V applied between the source and drain electrodes. $G_0 = 7.75 \cdot 10^{-5}$ S is conductance quantum.

The ambipolar CNT field effect transistor behavior had been obtained using the titanium contacts. Initially, the devices had very high interface resistance (on the order of 1 M Ω). Annealing such devices at 230 $^{\circ}$ C for 30 minutes reduces the contact resistance to about 100 k Ω , reduces hysteresis, and smoothens the ambipolar behavior. A typical FET behavior for devices with Ti contacts before and after annealing is shown in Fig. 5 for sweeping the voltage in one direction.

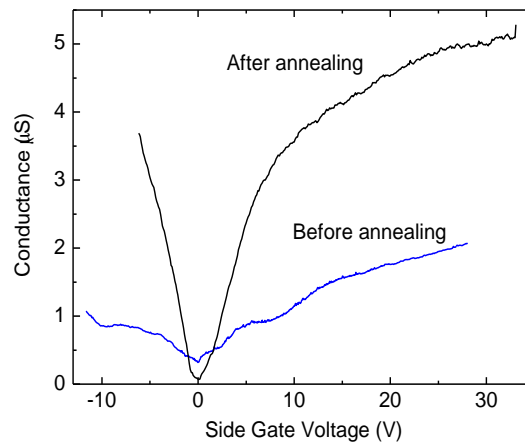


Fig. 5. Differential conductance of the CNT nano-circuit composed of the ambipolar field transistors with Ti source and drain electrodes before and after annealing.

The hysteretic behavior of the conductance vs. side gate voltage dependence with respect to direction of the voltage sweep (not shown in Fig. 5) can be attributed to defects (trapped charges or dipoles) that occur either at the interface between the CNT and the gate dielectric (interface defects) or at some position within the gate dielectric (bulk defects); see, e.g., Ref. (Kim, Javey et al. 2003, Jin, Islam et al. 2012). This hysteresis can be reduced or even eliminated by annealing as mentioned above.

Central result of this work is presented in Fig. 6 where the differential conductance $dI/dV(\Delta V) \equiv G_e(\Delta V)$ in units of microSiemens is plotted against the bias voltage across the CNT. In this device, the contacts were made of Ti (50 nm) annealed for 20 min at 270 °C, yielding the interface resistance of about 20 k Ω . The dependence displays hysteresis for different directions of sweeping the bias voltage. This type of hysteresis is not sensitive to annealing but instead strongly depends on the difference of the side gate potentials. We attribute the hysteretic behavior to manifestation of the energy levels localized in the central part C of the nano-circuit (cf. Fig. 2). Their position and width depends on the difference of the side gate potentials $V_{SG}^{right} - V_{SG}^{left}$, as is evidenced by respective features in the $G_e(\Delta V)$ curves (cf. Fig. 6). The features depend on a change ΔT of local temperature T versus direction of the electron current (cf. Figs. 2b and 2c). With an appropriate calibration, it allows for mapping the level shift ΔE and broadening Γ to the

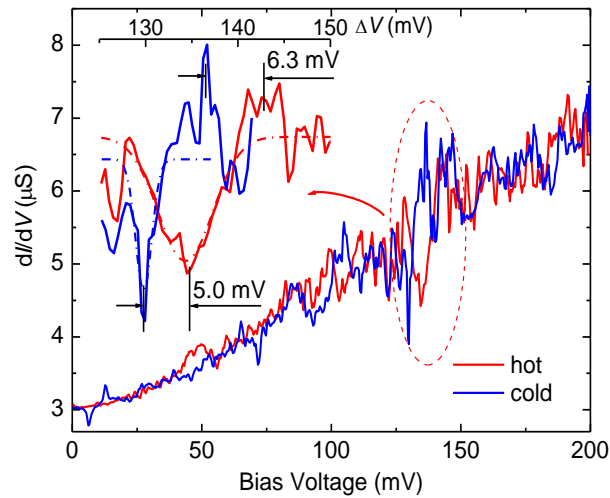


Fig. 6. Measured differential conductance $G_e(\Delta V)$ of the CNT thermoelectric circuit with Ti electrodes at the bath temperature of 77 K. Blue curve is for the cooling process sketched in Fig. 2b, whereas the red curve is for the heating process shown in Fig. 2c. Localized energy levels are identified as sharp features in the conductivity in the energy interval from 125 to 150 meV (marked by dashed line). A blowup of this region is shown in the inset. From the plot we find that $\Gamma_{cool} = 1.75 \pm 0.5$ meV and $\Gamma_{hot} = 5.6 \pm 0.7$ meV giving an estimate of $T_{hot} - T_{cold} \sim 114 \pm 7$ K.

temperature T of the active region. At $V_G^+ = 25$ V and $V_G^- = -3.5$ V for the curves in Fig. 6, the individual FET conductance was about 10.5 μ S. Individual FETs are 2 μ m each and the central part is 0.8 μ m. The entire length of the device was around 5 μ m. We used this circumstance to identify the energy levels localized in the active region C, as is shown in the inset of Fig. 6.

Discussion of the results. The obtained experimental data allowed us to determine the local intrinsic temperature change of the middle CNT region as follows. Because the local intrinsic temperature $T(x)$ depends on the coordinate x along the CNT axis, and the local resistance $R_{CNT}(T, x)$ of the CNT is temperature-dependent, this allows for identifying the energy levels E_C localized in the central

active region C from sharp features in the differential source-drain conductance curves $G_e(\Delta V)$. The local temperature is inferred by measuring the level width $\Gamma_{\text{cold(hot)}}$ and the shift ΔE_0 of the position of an energy level localized in the active central (C) region of CNT.

The temperature dependence $\Gamma_0(T)$ was derived by fitting the sharp features with the Gauss bell curves as was suggested earlier in Ref. (Yang, Fedorov et al. 2012). Comparing the $G_e(\Delta V)$ curves, measured at different V_{SG} corresponding to various local intrinsic temperatures T_c of region C, we identify the localized levels E_C whose position and width changes versus V_{SG} . The shifts $\Delta_{1,2}$ of the level positions occur owing to the electric resistance change of the active region C during the thermoelectric heating and cooling cycles. The sharp features in the $G_e(\Delta V)$ curve corresponding to energy levels E_C localized in the active region are shown in the inset of Fig. 6. A convenient sharp feature is the minimum of the $G_e(\Delta V)$ curve visible in Fig. 6. One can notice that the width $\Gamma_{\text{hot(cold)}}$ of the mentioned minimum is significantly different for the red (hot) and blue (cold) curves, i.e., $\Gamma_{\text{hot}} \gg \Gamma_{\text{cold}}$. By fitting the experimental data with the Gauss bell curves (dash-dotted curves in the inset of Fig. 6) we find $\Gamma_{\text{cool}} = 1.75 \pm 0.5$ meV and $\Gamma_{\text{cool}} = 1.75 \pm 0.5$ meV where the corresponding fitting error $\Delta\Gamma$ is determined by the number of experimental points used for averaging. The large magnitude of $\Delta\Gamma$ is caused by a considerable noise level during the measurement. The mapping of the level width $\Gamma_{\text{hot(cold)}}$ to the intrinsic temperature $T_{\text{hot(cold)}}$ of the active region is accomplished by determining the dependence of the level width $\Gamma_0(T_{\text{bath}})$ versus the bath temperature T_{bath} from the $G_e(\Delta V)$ curves measured when setting $V_{\text{SG}}=0$. The steady-state temperature dependence $\Gamma_0(T_{\text{bath}})$ is then used for calibrating the local temperature T_c at finite V_{SG} (Yang, Fedorov et al. 2012).

Our experimental results suggest that the electric current along the nanotube induces an impressive change of local temperature $\pm\Delta T = 57 \pm 6$ K inside the central CNT section. Depending on the direction of the source-drain current, the temperature either increases from the liquid nitrogen temperature $T = 77$ K up to $T_{\text{hot}} \approx 134 \pm 8$ K, or decreases from $T = 77$ K down to about $T_{\text{cold}} \approx 20 \pm 6$ K, thus evidencing a strong thermoelectric effect. We determine the dimensionless figure of merit ZT_{cold}^2 using a condition that the maximum temperature change ΔT_{max} is defined by $\Delta T_{\text{max}} = G_e s^2 T_{\text{cold}}^2 / (2\Lambda) = ZT_{\text{cold}}^2 / 2$, giving an impressive value $ZT_{\text{cold}} = 2\Delta T_{\text{max}} / T_{\text{cold}} \approx 5.6 \pm 1.7$ for our nano-circuit. Estimated cooling power density $P_{\text{cooling}} \sim 80$ kW/cm² for our CNT Peltier cooler where $R_{\text{contact}} \sim 100$ k Ω with CNT/Ti contacts. The overall cooling power can be considerably increased with scaling up to large CNT networks and arrays.

Temperature monitoring on nanoscale. Monitoring of intrinsic temperature and control of the heat flow allows for the study of energy transformations and for the ability to minimize the dissipation on the nanoscale. The energy losses caused by electric current are a fundamental obstacle which hampers the overall functionality of nano-circuits. This is due to the excessive heating. Electric signals, when controlled by elements of nano-electronic circuits, generate Joule-Lenz heat, thereby raising also the intrinsic temperature T on the nanoscale. Since the dimensions of the elements in the nano-circuit are small (relative to cross-section area S), the high current density J/S causes a large local Joule-Lenz heating. Excessive heating due to energy dissipation

not only impairs the performance of the nano-electronics elements, but can damage or even destroy them. In recent years, because of the wide spread implementation of high-density circuits, local

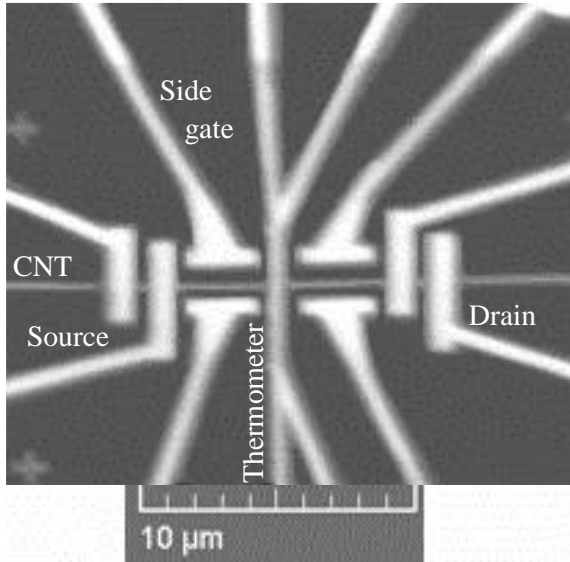


Figure 1: Single CNT Peltier cooler: two ambipolar CNT field-effect transistors (FET) connected in series.

overheating of nano-elements has become an acute issue. Another fundamental aspect of the same problem is that the thermal flow consists of three separate components: electrons, holes, and phonons. Therefore controlling the heat flow can be achieved by controlling/filtering out the effects from these components. For instance, when designing the nano-circuits, frequently there is a need to separate the flow of charged excitations from the flow of phonons, or shield a certain element thermally while retaining electric contacts. It helps to carry out the heat from a circuit element away, improving its functionality.

Thus, monitoring of the local intrinsic temperature T along with the thermal management are critical issues in determining viability of the nano-scale applications. Prevention of excessive heating is accomplished using a special geometry for the nano-circuits and implementing advanced semiconducting materials with large thermal conductance Λ . In this respect, carbon-based low-dimensional materials like carbon nanotubes (CNTs) and graphene along with atomic monolayer dichalcogenides, which are characterized by large $\Lambda=50-6000$ W/mK, are promising candidates. Implementing such nano-devices allows for reducing the local heating of the nano-circuit elements, thereby boosting their overall performance.

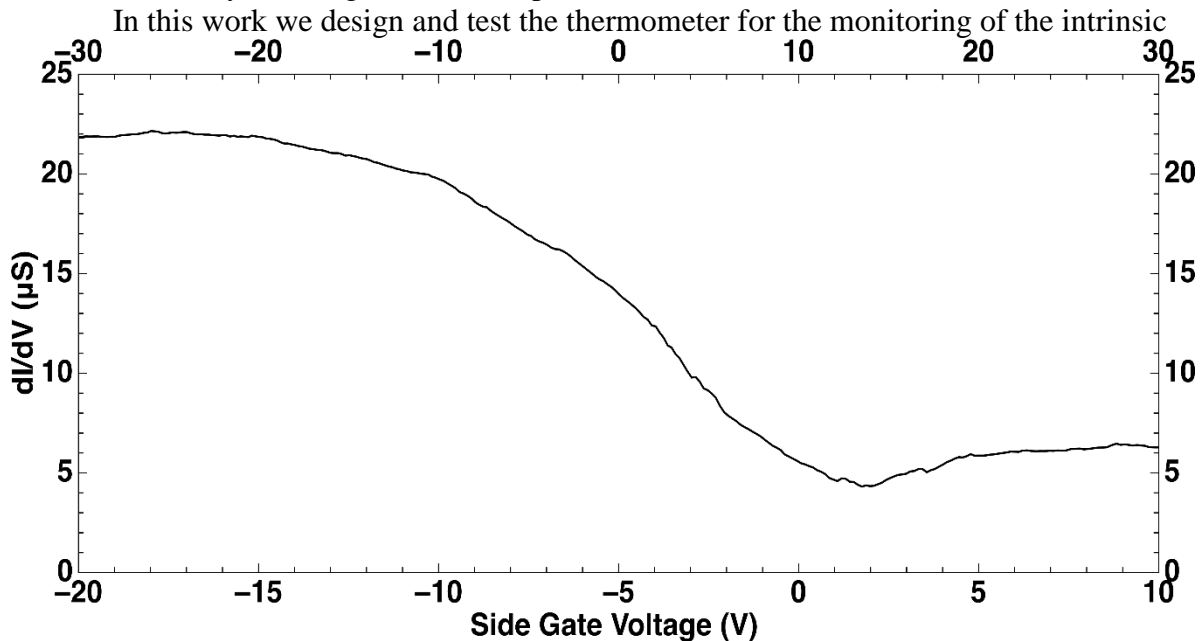


Figure 2: A graph of the conductance versus side-gate voltage of a single CNT device with Ti contacts after annealing

temperature in the carbon nanotube (CNT) thermoelectric circuits .

We consider a system where a semiconductor-type carbon nanotube is a central component (see Fig. 1). Two pairs of metallic (Ti) contacts to CNT and side gates form a nano-device which, from electric point of view, is a system of two field-effect transistors (SFTs) connected in series. In addition, a thermometer is placed in the center of the device, which we consider in a more detail below.

We also consider a bi-metal multilayer system used for the heat flow control in the nano-circuits. The bi-metal multilayer setup is used to filter the heat flow by separating the electron and phonon components one from another. The elements of the CNT nano-circuits form thermoelectric Peltier coolers based on ambipolar field effect transistors. In the devices, shown in figure 1, the concentration and polarity of the charge carriers are controlled by application of a local electric field, via side gate voltage. We have created a series of thermoelectric circuits using a variety of geometries and different metals to create gate, source, and drain electrodes. The field effect transistors (FET) were fabricated using conventional electron beam lithography techniques to pattern the source, drain, and gate structures on top of CVD grown CNTs. The CNTs of choice were characterized using AFM scanning techniques and the metallic structures were deposited in an electron beam evaporator. Excess tubes have been removed via an oxygen plasma etch thus preventing the sample leads from shorting together.

Initially the source and drain contacts were fabricated using a palladium/gold (3-5 nm)/(40 nm) multilayer where the Pd directly contacted the CNT. The Pd based devices exhibited a Pd/CNT interface resistance of 20 k Ω . Subsequently, this interface resistance was reduced to 4-6 k Ω via annealing in a hydrogen-argon atmosphere at 230 °C for 30 minutes. With the Pd contacts the CNT nano-circuits exhibited p-type FET behavior. The on state conductance was $.05e^2/\hbar$ whereas the off state conductance is negligible. Regardless of changes in annealing process and/or gate geometry (with some samples having less than 50 nm of separation between the CNT and side gate) we were unable to produce Pd contact devices with ambipolar behavior. This is likely due to palladium's high work function which creates a large barrier for incident electrons.

In order to achieve ambipolar behavior we have fabricated a series of samples that utilize a titanium layer to contact the CNT. These samples exhibit Ti/CNT interface resistances of 1 M Ω prior to annealing and display hysteric ambipolar behavior. After annealing using the same process as with the Pd contacts the interface resistance reduces to 40 k Ω , much of the hysteresis is eliminated, and the ambipolar behavior is smoothed. The post annealing gate behavior is shown in figure 2.

Furthermore, we have fabricated a number of nano-circuits. Our devices consists of two ambipolar CNT field effect transistors (FET) connected in series (see image of CNT PC with Ti source and drain electrodes on left panel). The conductance $G(V_G)$ of our ambipolar CNT FET versus side gate voltage V_G is shown in Figure 2. In the course of the work, the thermometer (see Figure 4 panel) which measures local changes in temperature was designed and fabricated.

In addition to all of the effort made to fabricate the CNT devices, there was a still a challenge that needed to be addressed in the measurements of these devices. In order to prove if these devices

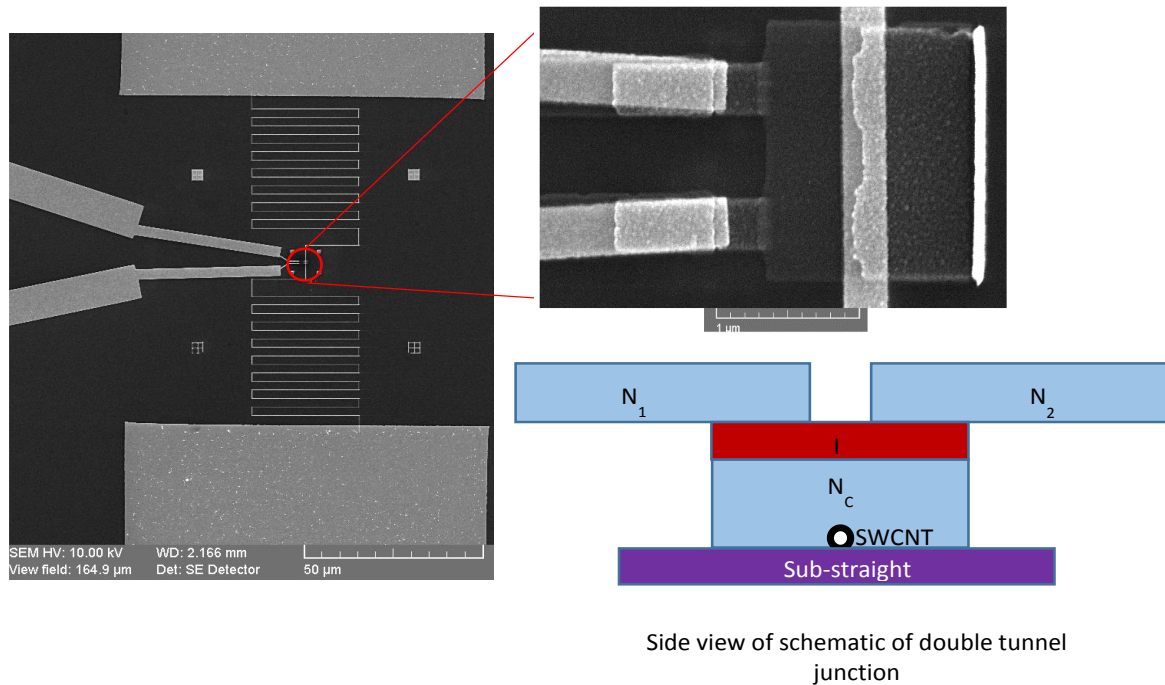


Figure 3: Left: Zoomed out SEM image of the test thermometer device. At the top and bottom of the image are the reservoirs for the meander which travels between. The left wires are the thermometer contacts. Top Right: Zoomed in image of the double tunnel junction used as a thermometer. The vertical wire is the meander which sits beneath the darker Al island. The horizontal wires on the left are Au contacts used to measure the double tunnel junction. These brighter horizontal lines are then connected to the central island by darker Al wires, evaporated using angled techniques. Bottom Right: A schematic representation of the double tunnel junction which will be used to measure the temperature of the CNT device. The temperature is determined from the conductance of this device from N₁ to N₂ bypassing the CNT.

work and further quantify the devices' characteristics, a measurement of the local temperature must be made. Since it must be a local measurement, the thermometer used must be fabricated onto the active portion of the device, restricting possible options. Additionally, the proposed device is to be tested at a large range of temperatures, so the thermometer must operate at the same temperature range. Finally, the temperature measurement must be non-invasive. The thermometer must be designed in such a way as to not be a heat leak into or out of the system. Therefore, the measurement must not use a lot of power (current) to prevent changing the local temperature due to heating.

In order to overcome these challenges, it was determined that a tunnel junction should be used as a thermometer for the following reasons. First, a tunnel junction is possible for in situ fabrication onto the CNT devices as currently designed. Second, since the devices are not conducting they will prevent heat leakage. Third, if designed correctly, they can be operated with a very small current that minimizes any interaction with the CNT device. Finally tunnel junctions have been shown to have a T^2 dependence with conductance, providing the possible sensitivity needed to see any temperature changes provided by the CNT device .

Before such a device could be implemented as a usable thermometer, the concept had to be turned into a standardized measurement device. The test thermometers were fabricated using e-beam lithography on a silicon sub-straight with a 300 nm thermally grown oxide layer. A gold meander (a long gold wire) is first placed onto the sample set between two thermal reservoirs. It will then be possible to model the meander's temperature profile for a given dc current. The known temperature profile will then allow the thermometer to be calibrated.

To test the double tunnel junction thermometers, the differential conductance of the thermometer (through the double tunnel junction only) was measured (using standard lock in techniques) from room temperature to liquid nitrogen temperatures. The results in figure 6 are consistent with those found by Koppinen .

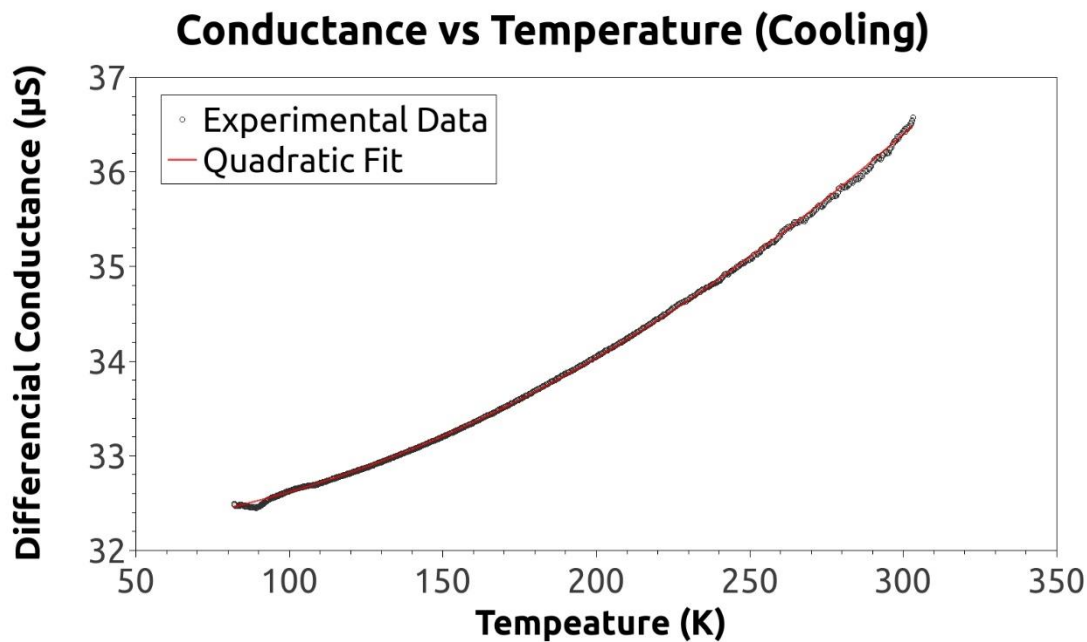


Figure 4: Black data is the conductance versus temperature graph for a double tunnel junction from room temperature to liquid nitrogen temperatures. The red line is a T^2 fit dependence as seen by other groups (Gloos, Koppinen et al. 2003).

The thermometer is fabricated using a double aluminum-aluminum oxide tunnel junction. These junctions are fabricated on top of the gold meander by using angled e-beam evaporation. First the central aluminum island is evaporated onto the meander (when the sample is perpendicular to the evaporation source). Without breaking vacuum, the aluminum is then oxidized. Aluminum oxidizes on the surface only, creating a small insulating layer on top of the island. Without breaking vacuum, a second layer of aluminum is then evaporated at an angle (55 degrees) on top of the aluminum island, creating the double tunnel junction. This geometry allows the middle island to thermalize with the gold meander (and later the CNT device), while the oxide layer provides the tunnel barrier, which thermally insulates the island from the thermometer leads. The last layer of aluminum then provides the tunnel contacts, such that small currents can pass through the island without passing it through the gold meander (altering the potential calibration).

Filtering the heat flow using a bi-metal multilayer setup. Along with the problem of direct temperature monitoring, in this work we studied also another relevant issue which is the control of the heat current. We consider a bi-metal multilayered structure depicted in Fig.5a representing the electric/heat conductance valve. The suggested system is intended to separate different components of the heat current, consisting of the flow of charged excitations and the flow of phonons. Such a multilayered system might be implemented, e.g., to insulate individual circuit elements thermally, while preserving the electric contacts. We performed analytical and numeric modelling of the propagation the heat through multilayered metallic stacks. The random layer thickness change is introduced to eliminate resonance transmission of phonons. Thus, the phonon flow across the multilayer is greatly reduced due to the low transmission probability $\zeta \ll 1$. However, the contribution of phonons to the heat transfer might exceed the contribution due to the electrons and holes. The multilayer actually acts like a filter for the two components of microscopic heat transport.

The heat flow filtering mechanism is understood within a simple analytical model. The multilayer represents a sequence of bilayers shown in Fig. 5a where metallic layers A and B are characterized by different Fermi velocities ($v_F^{A,B}$) and sound velocities ($s_{A,B}$). The phonon heat conductance through the multilayer Λ_{ph} is obtained from the Landauer formula (Gloos, Koppinen et al. 2003). One writes

$$\Lambda_{\text{ph}} = \frac{1}{2\pi(T_{\text{H}} - T_{\text{C}})} \int_0^{\infty} \hbar\omega\zeta_{\omega}(N_{\omega}^{\text{H}} - N_{\omega}^{\text{C}})d\omega$$

where $T_{\text{H,C}}$ and $N_{\omega}^{\text{h,c}}$ are the temperatures and the Bose-Einstein distribution functions in the "hot" and "cold" ends. The phonon transmission probability ζ_{ω} is obtained by the mode matching method (Gloos, Koppinen et al. 2003). If the temperature gradient across the junction is small, $T_{\text{H}} - T_{\text{C}} \ll T_{\text{H}} + T_{\text{C}}$, and the junction is ideally transparent for phonons, $\zeta(\omega)=1$, Λ_{ph} is quantized (Yamamoto and Watanabe 2006) as $\Lambda_{\text{ph}} \approx M(\pi^2 k_{\text{B}}^2 T / 3h)$ where M is the number of acoustic modes. For $L=1 \mu\text{m}$ and $w=20 \text{ nm}$ one roughly gets $\Lambda_{\text{ph}}=(50-6000) \text{ W}/(\text{m} \cdot \text{K})$.

Electron transport through the metallic multilayer is determined by the corresponding electrons (\mathbf{T}_{el}) and phonons (ζ) transmission probabilities. We compute \mathbf{T}_{el} and ζ in terms of the S-matrix method (Datta 1997). The electron S-matrix of the whole ABA ... B multilayer is composed of elementary blocks ABA. Here we assume that there are no interface A/B-barriers separating the A and B layers. The electron (hole) transmission (t_{ABA}) and reflection (r_{ABA}) coefficients which are the S_{ABA} matrix elements are obtained from the A/B-interface boundary conditions as (see, e.g., Refs. (Yamamoto and Watanabe 2006))

$$t(k_A, k_B) = 2ik_A k_B / \mathbf{D}_{k_A, k_B}$$

$$r(k_A, k_B) = (k_A^2 - k_B^2) \sin(k_B L) / \mathbf{D}_{k_A, k_B}$$

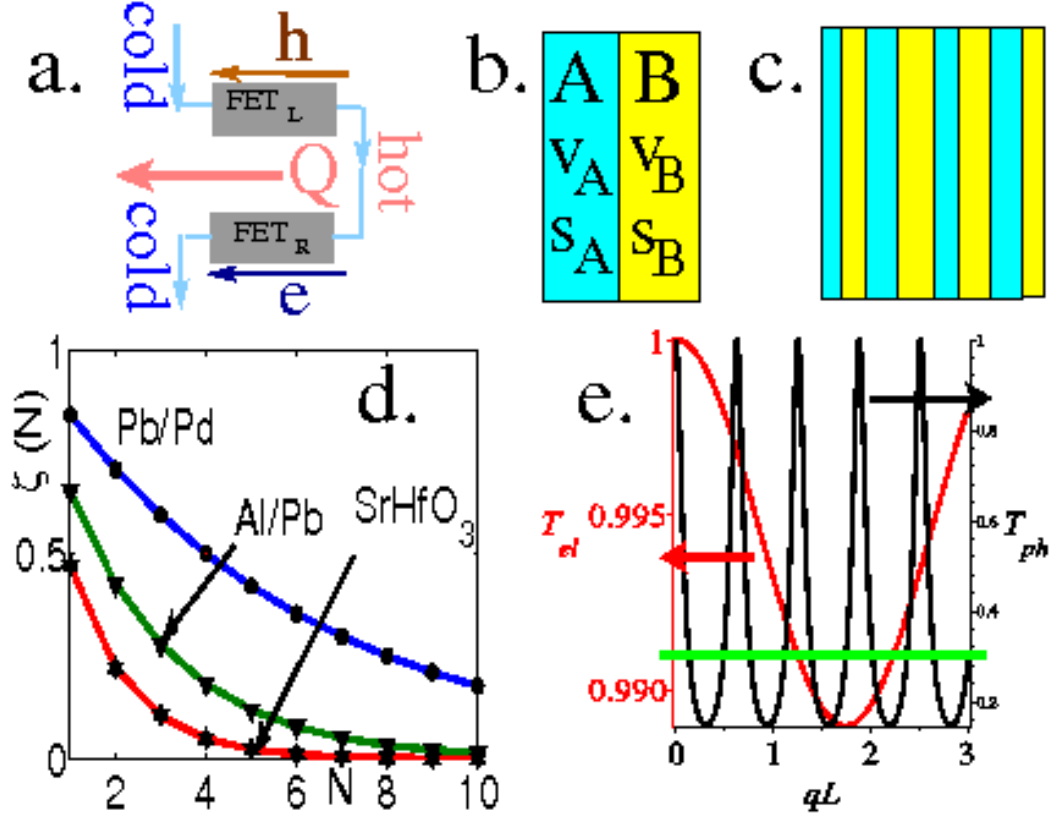


Figure 5: (a) Heat (Q) and electric (J) currents in the G-TEG involving the field effect transistors (FET_{L,R}). (b) Metallic bi-layer with $v_{AF}=v_{BF} \approx 1$ and $s_A=s_B \gg 1$. (c) Metallic multilayer with randomized layer thickness. (d) The two-scale plot for a single elementary ABA crank with the layer thickness $L_A=L_B=50$ nm and $\alpha=v_{AF}=v_{BF}=0.9$ (for electrons, black curve) on one hand and for $\alpha=5$ (for phonons, red curve) on the other hand. One may notice that phonons attenuate very strong while the electrons propagate almost free. The electrons correspond to $kL_{A,B} \ll 1$ while phonons to $qL_{A,B} \approx 10$. For such reason the effective electron transmission probability is practically ideal, i.e., $T_{el} \approx 1$ while the averaged phonon transmission probability $(\zeta)_q \approx 0.3$. Further suppression of the thermal phonon flow is accomplished by forming the sequence of N bilayers with a close but non-equivalent thickness around $L=50$ nm (for $T=10$ K). The phonon transmission through such a randomized Pb/Al-multilayer is not phase-coherent, thus the total phonon transmission probability is composed of corresponding probabilities for individual elementary bilayer blocks, i.e., $\zeta_{tot} \approx \zeta/N$ which already for, e.g., $N=6$ gives $\zeta_{tot} \approx 0.3/6 = 0.05$ while $T_{el}^{tot} \approx (T_{el})^5 \approx 1$, i.e., it remains nearly ideal. The last example illustrates the principle of the heat flow filtering: The electron and hole carry the heat free while the phonon thermal conductance almost vanishes across the Pb/Al multilayer. (e) The phonon transmission coefficient ζ for multilayered metallic electrode versus the number of layers N .

where the denominator is $\mathbf{D}_{k_A, k_B} = (k_B^2 + k_A^2) \sin(Lk_B) + 2ik_A k_B \cos(Lk_B)$, k_A and k_B are the electron wave vectors in A and B. Since the main contribution to \mathbf{S} and \mathbf{G} comes from the electron states near the Fermi level, one may use the linear dispersion law $E - E_F = \hbar v_F (k - k_F)$. Since the electron energy is conserved during the interlayer transmission, $E^A = E^B$ it gives $\hbar v_F^A (k^A - k_F) = \hbar v_F^B (k^B - k_F)$ or $v_F^A k^A \approx v_F^B k^B$. This allows rewriting the above equation simply as

$$t_a = 2i\alpha / \mathbf{D}_\alpha$$

$$r_a = (\alpha^2 - 1) \sin(\alpha) / \mathbf{D}_\alpha$$

where now $\mathbf{D}_\alpha = (1 + \alpha^2) \sin \alpha + 2i\alpha \cos \alpha$ and $\alpha = v_F^A / v_F^B$. The corresponding phonon transmission and reflection coefficients are derived in a similar way.

A very interesting consequence of the above formula takes place when $\alpha \approx 1$ for electrons while simultaneously $\alpha \gg 1$ for phonons. Such situation takes place, e.g., when one of the metals in the elementary bilayer is lead (i.e., A=Pb) while another metal is aluminum (B=Al). The Fermi velocities for the lead and aluminum are very close ($v_F^{Pb} = 1.83 \times 10^6$ m/s and $v_F^{Al} = 2.3 \times 10^6$ m/s respectively) while the sound velocities in the two metals are quite different (i.e., $s_{Pb} = 1158$ m/s and $s_{Al} = 6420$ m/s). This gives a big difference between the two ratios $\alpha_{el} = v_F^{Al} / v_F^{Pb} = 0.8$ on one hand while $\alpha_{ph} = s_{Al} / s_{Pb} = 5.5$ on the other hand. The whole ABA ... AB multilayer is then composed as a sequence of bilayers with randomly changing thickness. As is evident from Fig. fig1A-A c, the electron transmission probability through the whole metallic multilayer shown in Figs. 2c, fig1A-A a,b is nearly ideal, $T_{el} \approx 1$ while the phonon transport is practically blocked since $T_{ph} \ll 1$.

Since the lattice constants of the two metals A and B differ, there is a lattice strain immediately at the layer's A/B-interfaces. However, the strained region involves just a few atomic layers at the Pb/Al or Pb/Sn interfaces. Therefore the strain affects just on a tiny fraction of the whole multilayer's volume. Contribution of that strained region into the electron and phonon transport across the metallic multilayer is negligible if the length of the strained region in lateral direction is much shorter than the metallic layer thickness or/and the electron and phonon mean free paths. Similar metallic multilayers had been widely used in the superconducting junction technology and it is well known the interface strains do not impact the lateral electron transport. That happens because it acts just like a scatterer which size is less than 1 nm, i.e., it is much narrower than the phonon's wave length of interest which exceeds 10 nm for $T > 300$ K. The strained region is too narrow to change the electron band structure on the local scale < 1 nm. The local short scale lattice deformation < 1 nm is also unable to generate an electrostatic potential barrier for the electrons propagating in the lateral direction.

The difference in transmission probabilities of the electrons and phonons through the metallic multilayer can be exploited to filter the heat transport components: The electrons and holes propagate through the metallic multilayer almost free while the phonon transport is considerably reduced. Using the bimetal multilayers allows to reduce the overall high thermal conductance Λ_{ph} due to propagating the phonons in carbon nanotubes. This eliminates another obstacle to achieving a noticeable TEG efficiency. We strongly reduce Λ_{ph} , e.g., by connecting the carbon nanotube in a sequence with a material which Λ_{ph} is very low whereas the electron part, Λ_e , is high. Here decimating the phonon part of heat conductance is accomplished by connecting the carbon nanotube in a sequence with a multilayered valve pad. A multilayer with random layer thickness had been also considered by authors of Ref. (Yamamoto and Watanabe 2006) who studied a set of semiconducting layers with random thickness where energy gaps in the phonon spectrum are formed. However there are inherent controversies in that approach (Yamamoto and Watanabe 2006). In the multilayers with random thickness of semiconducting layers the energy gaps in the phonon spectrum are formed. Since the phonon gaps in distinct layers are positioned at different phonon energies, the resulting phonon heat conductance is strongly suppressed. Although it is supposed to improve ZT , the idea (Shafranjuk 2009) fails to work. The contradiction originates from two controversial inherent requirements. Namely, if the semiconducting layers are strongly coupled, the electric conductance and Seebeck coefficient are big. On the other hand, a strong interlayer coupling eliminates the phonon gaps since series of strongly coupled layers behave like a monolithic material where the phonon gaps vanish. As a result the phonon heat conductance Λ_{ph} is not being suppressed. In the opposite limit, when layers are weakly coupled,

the phonon gaps are indeed formed, causing the phonon heat conductance being suppressed. But an adverse effect is that the electric conductance and Seebeck coefficient are diminished with it also, because they are proportional to the interlayer coupling strength. In either case, weak or strong interlayer coupling, the figure of merit cannot be improved considerably by using the method of Ref. (Musho and Walker 2011). Our approach is based on a different idea which is more suitable for the TEG optimization. First, we consider *metallic* multilayer with ideally transparent interfaces. The metals have a much higher DOS than the semiconductors do. Besides, the metal/metal interfaces are very transparent for electrons. Therefore the lateral electric conductance and Seebeck coefficient through the multilayer is much higher than of the semiconducting multilayer with decoupled layers as in Ref. (Musho and Walker 2011). A critical distinction is that we use two metals A and B with similar Fermi velocities $v_{AF} \simeq v_{BF}$ but with very different sound velocities $s_A \ll s_B$ (e.g., Pb/Al or Pb/Sn). It yields a strong reduction of the phonon thermal conductance Λ_{ph} without sacrificing the electron transport coefficients. In this way we are considerably improving the TEG figure of merit. Another benefit of using the metallic multilayer instead, e.g., the semiconducting multilayer (Musho and Walker 2011) is that the much higher DOS in metals much better matches the high DOS in the HCF peaks. Because the electron part of the heat flow Q_{el} is strongly increased while the phonon part of the thermal flow Q_{th} is diminished, ZT is boosted 7 by orders of magnitude.

The phonon part of the thermal transport through the TEG had been examined as follows. We describe the non-equilibrium heat flow through the \mathbf{G} -stripe in presence of multiple scattering on lattice defects, boundaries, and electrons. A finite temperature difference δT between the opposite ends of each \mathbf{G} -stripe induces the thermal flow given as a sum of contributions of the individual phonon subbands. The phonon density of states $F_{\beta}(\omega)$ related to the phonon subband β is mismatched in adjacent layers of the H electrode sketched in Fig. 2c. Inside the \mathbf{G} -stripe, the phonon distribution function $N(\omega)$ is non-equilibrium which means that $N(\omega)$ deviates from the Bose-Einstein distribution in the hot (H) and cold (C) ends. For a "clean" carbon nanotube, the phonon mean free path exceeds the \mathbf{G} -stripe length L . Therefore the non-equilibrium effect does not influence the final results. The equilibrium phonon distribution at the \mathbf{G} -stripe ends is established due to a free phonon diffusion into the bulk of attached metallic contacts and dielectric substrate. The thermal conductance $\Lambda_{\mathbf{G}}^{\text{ph}}$ of the \mathbf{G} -stripe had been computed by using the phonon density of states $F_{\beta}(\omega)$ preliminary obtained for each phonon subband β .

The thermoelectric characteristics are found by solving the Dirac equation for chiral fermions in the carbon nanotube (see above). The analytical model is verified by numeric calculations based on the density functional theory. The electron and phonon excitation spectra are obtained considering influence of the inelastic electron-phonon and elastic electron-impurity scatterings. They are taken into account along with processes of the electron tunneling through the interface barriers. The electron-impurity and electron-phonon scatterings are included within the Keldysh-Green function technique which allows deriving of the quantum kinetic equations. We conclude that the suggested approaches of the intrinsic temperature monitoring combined with the heat flow management have a great potential for countering of the overheating problem in the nano-circuits. On the one hand, the double tunnel junction thermometer, designed and tested in the course of this work, performs the real time monitoring of the local temperature on the nano-scale. On the other hand, the suggested in this work the bi-metal multilayer structure minimizes the phonon component of the heat flow, while preserving the electronic part of it. Those approaches, if implemented, can greatly improve the overall efficiency (the figure of merit) of thermoelectric

devices converting the heat energy to electricity and vice versa or when implemented in the electronic nano-circuits to minimize of overall Joule Lenz energy losses. Besides, similar method can be used to counter the Joule Lenz overheating of large nano-circuits.

Giant thermoelectric effect in graphene stripes with heavy chiral fermions. A conversion of thermal energy into electricity was considered in the electrically polarized graphene stripes with zigzag edges where the heavy chiral fermion (HCF) states are formed. The stripes are characterized by a high electric conductance G_e and by a significant Seebeck coefficient S . The electric current in the stripes is induced due to a non-equilibrium thermal injection of “hot” electrons. This thermoelectric generation process might be utilized for building of thermoelectric generators with an exceptionally high figure of merit $Z\delta T \gg 1$ and with an appreciable electric power densities ~ 1 MW/cm².

Theoretical study of the thermoelectric phenomena in conditions of the quantum Hall effect. Another relevant activity in the course of the project was our work on quantization of the magneto-thermoelectric transport occurring when an external d.c. magnetic field is applied to the C/N-knot formed as crossing between a narrow stripe of conducting atomic monolayer C on the one hand and metal stripe N on the other hand. The temperature gradient in C is created by injecting the non-equilibrium electrons, holes and phonons from the heater H thereby directing them toward the C/N-knot. A non-linear coupling between electron states of the C/N-knot counter electrodes causes splitting of the heat flow into several fractions owing to the Lorentz force acting in the C/N-knot vicinity, thereby inducing the magneto-thermoelectric current in N whereas the phonons pass and propagate along C further ahead. The heat flow along C generates a transversal electric current in N showing a series of maximums when dimensions of the Landau orbits and the C/N-knot match each other. It allows observing the interplay between the quantum Hall effect and the spatial quantization.

Conclusions. To summarize the work thus far, we studied a highly efficient mechanism of Peltier cooling taking place in the carbon nanotube thermoelectric nano-circuits. The appreciable densities of cooling power $P_{\text{cooling}} \sim 80$ kW/cm² can be increased further using the voltage-controlled spectral singularities and filtering the electric/heat currents, as suggested in Refs. (Musho and Walker 2011).

Future's planes. The suggested approach of Peltier cooling has a great potential for a variety of applications. Obtained figure of merit $ZT_{\text{cold}} = 7.5$ are increased further by an order of magnitude using the source and drain contacts with higher transparency. For instance, the Ti gates and contacts can be replaced with Pd and Ni electrodes providing much higher transparency of the metal/CNT interfaces. Additional improvements of the thermoelectric circuit performance can be accomplished using the bi-metal multi-layer electrodes allowing filtering of the heat flow. We anticipate that the aforementioned additional measures will result in improvement of the figure of merit with order of magnitude up to $ZT_{\text{cold}} = 100$. Peltier nano-coolers with a huge figure of merit $ZT_{\text{cold}} = 100$ and the cooling power $P_{\text{cooling}} \sim 1$ MW/cm² can revolutionize the nanoelectronics, since they provide cooling from the room temperature T_{room} down to the liquid helium temperature T_{He} on the nanoscale. Furthermore, it would make possible the creating of room-temperature superconducting nano-electronics when the circuit elements the all are refrigerated from T_{room} down to T_{He} .

Publications acknowledged support from the AFOSR grant FA9550-11-1-0311

Book: Serhii Shafraniuk, *Graphene: Fundamentals, Devices and Applications*, Pan Stanford Publishing, (Feb 28, 2015, 400 pages, on sale).

Referred journal articles

1. S. E. Shafraniuk, *Converting heat to electricity by a graphene stripe with heavy chiral fermions*, Eur. Phys. J. B (2014) 87: 99 DOI: 10.1140/epjb/e2014-40794-0.
2. Y. Yang, G. Fedorov, J. Zhang, A. Tselev, S. Shafraniuk and P. Barbara, (2014) *Search for superconductivity at van Hove singularities in carbon nanotubes*, In Carbon-based Superconductors: Chapter 2, Pan Stanford Publishing.
3. T. Gupta, I. P. Nevirkovets, and S. Shafraniuk, *Peltier cooling in carbon nanotube circuits*, (2015) *submitted*.
4. S. E. Shafraniuk, *Quantized magneto-thermoelectric transport in low-dimensional junctions*, (2014) *submitted*.
5. S. Mayle, T. Gupta, S. Davis, V. Chandrasekhar and S. Shafraniuk, *Thermometry and thermal management of carbon nanotube circuits*, (2015), *submitted*

References.

- Bell, L. E. (2008). "Cooling, heating, generating power, and recovering waste heat with thermoelectric systems." *Science* **321**(5895): 1457-1461.
- Berber, S., Y. K. Kwon and D. Tomanek (2000). "Unusually high thermal conductivity of carbon nanotubes." *Physical Review Letters* **84**(20): 4613-4616.
- DiSalvo, F. J. (1999). "Thermoelectric cooling and power generation." *Science* **285**(5428): 703-706.
- Dubi, Y. and M. Di Ventra (2011). "Colloquium: Heat flow and thermoelectricity in atomic and molecular junctions." *Reviews of Modern Physics* **83**(1): 131-155.
- Finch, C. M., V. M. Garcia-Suarez and C. J. Lambert (2009). "Giant thermopower and figure of merit in single-molecule devices." *Physical Review B* **79**(3).
- Gloos, K., P. J. Koppinen and J. P. Pekola (2003). "Properties of native ultrathin aluminium oxide tunnel barriers." *Journal of Physics-Condensed Matter* **15**(10): 1733-1746.
- Jin, S. H., A. E. Islam, T. I. Kim, J. H. Kim, M. A. Alam and J. A. Rogers (2012). "Sources of Hysteresis in Carbon Nanotube Field-Effect Transistors and Their Elimination Via Methylsiloxane Encapsulants and Optimized Growth Procedures." *Advanced Functional Materials* **22**(11): 2276-2284.
- Kim, W., A. Javey, O. Vermesh, O. Wang, Y. M. Li and H. J. Dai (2003). "Hysteresis caused by water molecules in carbon nanotube field-effect transistors." *Nano Letters* **3**(2): 193-198.
- Musho, T. D. and D. G. Walker (2011). "Thermoelectric properties of superlattice materials with variably spaced layers." *Journal of Materials Research* **26**(15): 1993-2000.
- Pop, E., D. A. Mann, K. E. Goodson and H. J. Dai (2007). "Electrical and thermal transport in metallic single-wall carbon nanotubes on insulating substrates." *Journal of Applied Physics* **101**(9).
- Reddy, P., S. Y. Jang, R. A. Segalman and A. Majumdar (2007). "Thermoelectricity in molecular junctions." *Science* **315**(5818): 1568-1571.
- Shafranuk, S. E. (2009). "Reversible heat flow through the carbon tube junction." *Epl* **87**(5).
- Shafranuk, S. E. (2014). "Converting heat to electricity by a graphene stripe with heavy chiral fermions." *European Physical Journal B* **87**(4).
- Small, J. P., K. M. Perez and P. Kim (2003). "Modulation of thermoelectric power of individual

carbon nanotubes." Physical Review Letters **91**(25).

Yamamoto, T. and K. Watanabe (2006). "Nonequilibrium Green's function approach to phonon transport in defective carbon nanotubes." Physical Review Letters **96**(25).

Yang, Y. F., G. Fedorov, J. Zhang, A. Tselev, S. Shafranjuk and P. Barbara (2012). "The search for superconductivity at van Hove singularities in carbon nanotubes." Superconductor Science & Technology **25**(12).